Manuscript title page

1. Manuscript title: Contribution of the axon initial segment to action potentials recorded extracellularly.

2. Abbreviated Title: Impact of AIS on extracellular action potentials.

3. Author names and affiliation, including postal codes:

Maria Teleńczuk, Unité de Neurosciences, Information et Complexité, CNRS, 91190 Gif-sur-Yvette, Paris

Romain Brette, Sorbonne Universités, UPMC Univ Paris 06, INSERM, CNRS, Institut de la Vision, 75012 Paris, France

Alain Destexhe, Unité de Neurosciences, Information et Complexité, CNRS, 91190 Gif-sur-Yvette, Paris

Bartosz Teleńczuk, Unité de Neurosciences, Information et Complexité, CNRS, 91190 Gif-sur-Yvette, Paris

4. Corresponding author with complete address:
Bartosz Teleńczuk, Unité de Neurosciences, Information et Complexité, CNRS, 91190 Gif-sur-Yvette, Paris
e-mail: telenczuk@unc.cnrs-gif.fr

5. Number of pages: 35
6. Number of figures: 12
7. Number of Tables: 0
8. Number of Multimedia: 0
9. Number of words for Abstract: 147
10. Number of words for Introduction: 650
11. Number of words for Discussion: 841

12. Conflict of Interest: Authors report no conflict of interest

13. Acknowledgements: Research supported by the CNRS, the European Union (Human Brain Project H2020-720270), and the Agence Nationale de la Recherche (ANR-14-CE13-0003). MT was supported by Ecole des Neurosciences de Paris (ENP, http://www.paris- neuroscience.fr/) and DIM Cerveau et Pensée (http://dimcerveaupensee.fr/).

Abstract

Action potentials (APs) are electric phenomena that are recorded both intracellularly and extracellularly. APs are usually initiated in the short segment of the axon called the axon initial segment (AIS). It was recently shown that at onset of an AP the soma and the axon form a dipole. We study the extracellular signature (the extracellular action potential, EAP) generated by such a dipole. First, we demonstrate the formation of the dipole and its extracellular signature in full morphological models of a reconstructed pyramidal neuron. Then, we study the EAP waveform and its spatial dependence in models with axonal spike initiation and contrast it with the EAP obtained in models with somatic AP initiation. Finally, we discriminate the EAP at short distances from the neuron (near field) and at long distances (far field). Our study has consequences for interpreting extracellular recordings of single-neuron activity and determining electrophysiological neuron types, but also for better understanding the origins of the high-frequency macroscopic electric fields recorded in the brain.

Significance Statement

Action potentials in most neurons initiate in the axon initial segment (AIS). However, AIS is often neglected in computational studies. We studied the consequences of this initiation mechanism on the extracellular signatures of action potentials. By means of computer modelling we show that AIS forms

a dipole with the soma. In addition, the amplitude of the extracellular action potential (EAP) generated by this dipole changes little with soma-AIS distance while the width of the EAP increases with the soma-AIS distance. This may help to monitor dynamic changes in the AIS position in experimental *in vivo* recordings.

Introduction

Action potentials (APs) are the main output of neuronal computation arising due to neuronal membrane excitability. The most direct method to detect APs is by intracellular recordings for which a glass pipette is inserted into the soma. Extracellular recordings are gaining much popularity thanks to the possibility of massive recordings from large samples of neurons (Jun et al., 2017; Stevenson and Kording, 2011). However, such methods offer little insight about the type of neuron the AP originates from. One possible approach uses the AP waveshape to discriminate between discrete neuronal types from extracellular recordings (Barthó et al., 2004). The accuracy of these methods was confirmed by functional interactions between pairs of neurons (Peyrache et al., 2012), but the direct mapping between neuron type and its extracellular waveshape needs a detailed model of how the latter is generated.

On the other hand, APs can also contribute to the local field potentials and electroencephalograms recorded far from the neuronal source. In partic-

ular, the high-frequency components of these signals can relate to the firing rates of large population of neurons (Reimann et al., 2013). These high-frequency local field potentials are also known to be sensitive to the neuronal responses at single neuron and single trial level (Telenczuk et al., 2015). Therefore, modelling of action potentials can be as important as modelling of the passive dendritic and synaptic currents for understanding the LFP or EEG and in particular their high-frequency components.

The extracellular signature of APs has been a topic of computational studies (Bédard et al., 2004; Gold et al., 2006; Milstein and Koch, 2008). These studies emphasize the role of passive currents and dendritic compartments in the generation of the action potentials. However, in most of those models spikes were initiated in the soma neglecting the importance of the site of AP initiation.

In most neurons an AP initiates in the axon initial segment (AIS) (Stuart et al., 1997a; Stuart et al., 1997b). When measured intracellularly in the soma, the AP starts with a characteristic kink (Naundorf et al., 2007) that can be explained by the "critical resistive coupling model", according to which the AP is initiated through the strong resistive coupling between a small AIS and a large soma (Brette, 2013a; Telenczuk et al., 2017). Such an AP initiation is better explained by the critical resistive coupling hypothesis, which predicts that the AP is initiated due to the interaction between AIS and much larger soma. In this mechanism of AP initiation, AIS and soma create effectively a current dipole, which generate extracellular potential reflecting

the AP (Telenczuk et al., 2017).

We studied the contribution of the AIS-based initiation of AP to the extracellular field and its effect on the shape and amplitude of extracellular action potential (EAP). In particular, we studied realistic model neurons with AIS and modify the sodium channel density to initiate the AP in the soma. By means of computational modelling, we show that the AIS contributes significantly to the EAP. Although, the localization and length of the AIS have only a minor effect on the appearance of the AP recorded intracellularly from the soma, extracellularly the presence of AIS has a large impact on the shape of EAP. In addition, we show that the distance between the soma and AIS can have large impact on the EAP waveform.

In the far field, the AIS-soma distance has little impact on amplitude and shape of EAP. The far-field EAP can be best modelled by the dipole representing soma-AIS. The increase in the distance between soma and AIS is compensated by the inverse relationship between the intracellular current and this distance, so the dipole moment remains constant and hence does not produce measurable changes in the EAP amplitude (Hamada et al., 2016).

We believe that these findings improve our understanding of the close-field and far-field contribution of the AP to the electric fields in the brain. It will also help to interpret recordings of various signals ranging from the EAP, through LFP to EEG.

Materials and Methods

Full morphology model

We used full morphology model (physiological Na model) of the rat neocortex, layer 5 pyramidal neuron described in Hallermann et al. (Hallermann et al., 2012). Here, the authors gave particular care to fit parameters of all the channels to the experimental data leading to realistic current flow within and outside of the cell. Most importantly, in this model action potentials initiate in the axon initial segment as is the case in real neurons. The details of the model can be found in (Hallermann et al., 2012).

To compare the results of the original model to the neuron where the action potential initiation takes place in the soma, we reduced the density of the sodium channels in the axon initial segment to 480 $pS\mu m^{-2}$ throughout the length of the initial segment of the axon (70 μm) while density of the sodium channels in the soma remained the same (500 $pS\mu m^{-2}$, distribution of sodium channels throughout the axon initial segment, Fig. 2, reduced Na model). This was enough for an action potential to initiate in the soma. We note that there are less sodium channels in the altered model leading to lower current flow, therefore comparison of the crude amplitude of the potential might be misleading. This is why, where necessary, we normalized the data to the highest absolute value of the potential (Fig. 6).

To trigger the action potential we injected current to the soma. To remove signal associated with the current injection we removed all the active channels

from the model and stimulated it in the same way. We then subtracted the results of the passive model from the results of each of the active models.

In the model, in all the calculations, the soma is represented as a cylinder. However, in the Figures we represent it as a triangular shape for easier visualisation of the morphology of the cell.

Soma-axon model

We used a simple neuron consisting of a soma (20 x 30 μm, 6 segments) and an axon (1 x 50 μm, 10 segments), adapted from (Yu et al., 2008). Figure 9 (top left) shows the sample schematics of the shape of the neuron. The simulation was controlled from Python using the Neuron-Python interface (Hines et al., 2009).

Linear Source Approximation

To estimate the extracellular potential, we used the Linear Source Approximation (LSA) method, which calculates the summed potential generated by currents originating from line sources with known sizes and positions. This method is known to be more precise than approximating the currents by point sink and sources (Holt, 1997; Wilson and Bower, 1992). We then applied the LSA estimation to cylinders obtained from the segmentation by Neuron simulator (in total 16 cylinders, see above) (Hines and Carnevale, 1997). The field was calculated using the LSA implementation of NeuronEAP Python library

(Telenczuk and Telenczuk, 2016) which uses Linear Source Approximation to calculate the field generated by a neuron simulated in Neuron simulator. In all calculations we used an extracellular conductivity of 0.3 Sm^{-1}.

The current injected in the soma creates effectively a monopole in the extracellular potential producing a baseline shift in the extracellular potential. In Figure 9 we removed this baseline by calculating an average potential in a window of 2 to 1 ms before the peak of the action potential.

Results

Description of the model

To determine the contribution of an action potential to the electric field recorded around the neuron, we performed simulations of a detailed reconstruction of a thick-tufted pyramidal neuron (neocortex, layer 5, rat, Fig. 1). The morphology reflected real reconstructed neurons with all neuronal compartments including an axon and dendrites. The densities and the kinetics of sodium Na^+ and potassium K^+ channels in soma and axon were constrained by the experimental data. In particular, two different types of sodium channels were introduced (Na and Nax) with different voltage activation threshold and different distribution of the channel density across the axosomatic axis (Fig. 2, left). Overall, this model has been found to match well the properties of an action potential initiation of cortical neurons (Hallermann et al., 2012; Telenczuk et al., 2017).

AP is initiated in the AIS and gives a characteristic "kink" to the somatic potential

Importantly, in this model the action potential initiates distally from the soma, in the so-called axon initial segment (AIS), and later triggers a somatic AP which is in agreement with physiological recordings (Stuart et al., 1997a). This mechanism of AP initiation gives a characteristic "kink" at the onset of the somatic AP (Fig. 3A). This is due to a strong resistive coupling between the AIS and soma (Telenczuk et al., 2017). The resistive coupling model predicts that the soma and AIS forms a dipole at spike initiation, which should be observed in the extracellular electric field.

AIS generates positive peak at the beginning of the spike

We first analysed the EAP waveform associated with a single AP generated by the neuron. Previous modelling studies have indicated that mainly sodium currents in the soma and dendrites might contribute to the initial phases of the EAP, whereas later phases are shaped by the repolarisation mediated by potassium currents in these compartments (Gold et al., 2006). In contrast, axon and distal dendrites as well as capacitive current contribute little to the EAP. It is important to note that in those studies the action potential appeared almost simultaneously in the soma and AIS, i.e. it manifested somatic initiation of the AP (Brette, 2013b; Telenczuk et al., 2017).

We re-evaluated the contribution of the AP to the extracellular potential in the more realistic model with AIS-initiated AP. First, we calculated and

plotted the EAP recorded in the perisomatic area covering soma, proximal dendrites and the AIS in the physiological Na model (Fig. 4). As in Gold et al. (Gold et al., 2006) we found a large and sharp negative peak, due to sodium inflow, followed by a broad positive peak, due to potassium repolarisation of the soma and dendrites. Interestingly, in some electrodes (around and above soma) these peaks were preceded by a sharp positive deflection reflecting strong axial currents flowing between AIS and soma at the onset of the AP.

To confirm that this initial positive peak is related to the resistive coupling between soma and AIS forming a dipole, we lowered the densities of sodium channels in the AIS (Fig. 2, right). As expected, this modification lead to the somatic initiation of the AP, which appears simultaneously at soma and AIS (these two compartments being almost isopotential), and longer AP latency due to higher threshold (Fig. 3). The EAP waveforms obtained in this modified model lack the initial positivity consistently with the results of Gold et al. (Gold et al., 2006). We emphasise though that such a model is inconsistent with the experimental observation of the AP initiation, which support axonal (AIS) rather than somatic initiation of APs.

The AIS enhances the EAP amplitude at broad spatial ranges

The peak-to-peak amplitude decays with the distance from the neuron (Fig. 5). It is highest around soma and AIS, where the largest inflow of sodium and outflow of potassium during the AP takes place. Lowering sodium channel

density such that AP initiates somatically attenuates the peak-to-peak amplitude of the EAP, which is expected from the decrease of the total membrane current in the low-sodium model (not shown). Importantly, the reduction of EAP amplitude was most pronounced in the axonal region, especially in the proximity of the axon segment previously acting as the AIS (Fig. 6).

Next, we plotted the peak-to-peak amplitude of the EAP across four lines perpendicular to the somatodendritic axis (Fig. 5). Close to the neuron the profile of the EAP amplitude was non-monotonic due to the complex morphology of the neuron but it decreased proportionally to the inverse of distance from the source at larger distances (see also below). Again, due to the larger total membrane current the EAP amplitude is greater in standard sodium models compared to the low-sodium modification across all distances.

AIS and soma form a current dipole

In the original Hallerman et al. model (Hallermann et al., 2012) (physiological Na model), at the moment of the AP initiation the axial current from AIS to soma form a current loop together with the extracellular currents. This is similar to the currents generated in the so-called current dipole, where the AIS plays the role of the current sink and soma plays the role of the source (Fig. 7). This relation is reversed during the repolarisation phase of the AP (Telenczuk et al., 2017).

Such a configuration of a current source and sink generates a dipolar electric field (Fig. 7). This could be also observed in the current source

density (CSD) estimation, which shows a prominent sink around the AIS and source in the soma at the onset of an AP. The sinks and source are inversed at the later, repolarisation phase of the spike (Fig. 8). Due to the dipolar configuration the extracellular potential is highest in the proximity of either of the two "poles" (source or sink) and reverses around the center along the soma-AIS axis. A well-known approximation (Griffiths, 1999; Nunez and Cutillo, 1995) shows that at distances much greater than the separation between the source and sink, the electric potential decays according to the inverse square law (Fig. 5). This is in contrast to the extracellular field generated by an AP propagating along the axon (Stegeman et al., 1987), which forms a current source flanked at both sides by current sinks. Such a configuration can be observed in the nodes of Ranvier visible in the CSD map (Fig. 8). Such current distribution is well captured by the current quardupole model, which manifests inverse cubic dependence on the distance from the source. Consequently, the contribution of the AIS-soma dipole at larger distances is expected to be greater than the contribution from a local propagating (quadrupolar) AP.

Similarly, in the model with the somatic initiation of the AP (reduced Na model), soma and AIS are almost isopotential so no current flows between them and they contribute little to the EAP. In this case the dipole is rather formed between the soma and proximal dendritic tree (Fig. 8).

AIS-soma contribution can be approximated by a simple model of soma/AIS

The electric field obtained from the full morphological models contain a mixture of contributions from passive dendritic compartments and active axonal/somatic compartments giving rise to a complex configuration of current sinks and sources (as seen in the CSD map, Fig. 8). To isolate the effects of the soma-AIS dipole and its contribution to the far-field potential, we decided to further corroborate the consequences of the "critical resistive coupling" with a simplified electric dipole model. We reduced the model to a cylindrical soma and axon. All Na^+ and K^+ channels were placed in the AIS modelled as a 5-μm-long segment of the axon located 45 μm distally from the soma.

This model approximates well the dipolar field observed in the full morphological model described above (Fig. 7 and 8). The extracellular potential recorded at various locations spread over the vertical axis from the soma and decays with the inverse square of the distance as observed in the full morphology simulation (Fig. 9). The divergence between the reduced and full morphology model might be due to dendritic compartments that dominate EAP at low frequencies.

EAP amplitude weakly depends on the distance of AIS from soma

We modified the position of the AIS to investigate its impact on the amplitude and width of the EAP. In the simple dipole model, the amplitude of the

extracellular potential at fixed distance depends on the product between the dipole current (I, axial current between soma and AIS) and the separation between the poles (d, the distance from soma to the AIS; Fig. 10). Therefore, increasing the distance of the AIS might increase the amplitude of the EAP, but we found only weak dependence (Fig. 9). A possible reason is that in this model the axial current at the same time decrease with the inverse of the distance between AIS and soma and compensate for the (linear) increase in dipole length (Fig. 11) (Hamada et al., 2016).

To investigate the effect of the AIS position on the current intensity I, we measured the axial current during the action potential for varying positions of the AIS. We found that the amplitude of the axial current decreased with the inverse of the distance between the AIS and the soma (Fig. 11A). Indeed, the same Figure (Fig. 11B) shows that it is possible to fit a straight line of slope $a = -1$ through the points representing the logarithm of the maximum axial current versus the logarithm of the soma-AIS distance. This linear relation confirms that the amplitude of the axial current is inversely proportional to the distance between the soma and the AIS, $I \sim 1/d$. Such a relationship is also predicted by the resistive coupling hypothesis (Hamada et al., 2016). Since the far-field model of the extracellular potential predicts that the potential increases with the distance between source and sink, this trend should compensate for the drop of current magnitude shown in Figure 11. Therefore, the far-field approximation of the dipole model would predict no difference in the amplitude of the extracellular potential due to the AIS

position.

EAP broadens with AIS distance from soma

To study the effect of the AIS position on the extracellular action potential width, we calculated the extracellular potential generated by models with the AIS placed at ten different positions from the end of the soma, up to 45 μm distally. We observed that the extracellular action potentials become gradually wider with increasing distance between the soma and the AIS (Fig. 12B), while the shapes of intracellular waveforms remain similar (Fig. 12A, insets). The functional form of this dependence changes only slightly with the location of the recording site (Fig. 12B, dashed vs. solid line).

Discussion

Using full morphological models of reconstructed neurons and simplified soma-axon models we have shown that extracellular action potentials can be reconstructed from the current dipole formed by the soma and AIS at their initiation. By comparing the EAP at different locations close to the spiking neuron we also show that its shape depends on the position of the recording electrode with respect to the neuron promoting the extracellular contribution of different compartments of the neuron. In addition, while the width of the EAPs varies with the distance between the soma and the AIS, its amplitudes remains relatively constant.

The contribution of the AP to the extracellular field is shaped by the structure of the dendritic tree and the site of AP initiation. Large body of experimental data support the more distal initiation in the axon initial segment, but the impact of axonal initiation on the EAP had not been examined before. Using simplified models we showed that in the initial phase of the AP, the soma and AIS form a current dipole, whose contribution to the electric field decays inversely with the square of the distance from the dipole. At large distances (far-field approximation) the dipole contribution to the extracellular field does not depend on the separation between the AIS and the soma In contrast, the width of the EAP increases with the soma/AIS separation.

Our results provide an important insight into the understanding of EAPs. It is known that the shape and the amplitude of the extracellular action potentials vary depending on the location of the recordings (Gold et al., 2006). Also, different types of neurons display extracellular action potentials of different width, such as excitatory cells, which tend to have broader extracellular action potentials when compared with interneurons (Barthó et al., 2004; McCormick et al., 1985), although there are exceptions (Vigneswaran et al., 2011). To separate action potentials of multiple neurons recorded extracellularly, it is common to use the waveform features of an extracellular action potential, such as the half-widths of the positive and negative peaks, the interval between them and the difference of their amplitudes (Lewicki, 1998; Einevoll et al., 2012). In addition, these and other waveform features some-

times allow the identification of neurons of different types (Peyrache et al., 2012; Dehghani et al., 2016) . However, the significance of such features and their biophysical underpinnings are not completely understood. Numerical simulations of the extracellular field around reconstructed morphology of CA1 pyramidal neurons showed that the width of the extracellular action potential increases proportionally with the distance between the soma and the recording electrode (Gold et al., 2006). In addition, in this study the shape and amplitude of the extracellular potential was strongly affected by the channel densities in the dendrites and in the axon initial segment. In our work we show that the extracellular features of action potentials depend also on the exact location of their initiation site.

Finally, our results show that it should be possible, and of great interest, to follow experimentally the dynamic change of the AIS position by means of extracellular recordings. The length and distance of AIS from soma vary between neurons of same and different types (Fried et al., 2009; Kuba et al., 2006). Furthermore, the AIS is plastic and its length and position can change as a result of elevated activity which could occur due to plastic changes in a time scale of hours (Evans et al., 2015) to days (Grubb and Burrone, 2010; Evans et al., 2013; Muir and Kittler, 2014). This also happens as a consequence of a diseased state such as a stroke (Hinman et al., 2013; Schafer et al., 2009). Therefore, we expect that the shape of the EAP will vary according to the position of the AIS, such that long-term recordings from the same neuron could show gradual increase of the AP width. Since,

the plasticity of AIS was never studied *in vivo* from intact neurons, this may open new methods of visualising such dynamic changes and investigating their functional role.

At the population level, the contribution of neurons to the local field potential (LFP) depends critically on the presence of voltage-dependent channels and neuronal morphology. For example, during the up state the LFP contains larger contributions from the active potassium and sodium currents than from synaptic currents (Reimann et al., 2013); similarly active conductances in the dendrites were shown to have major impact on the spectrum of the field potential (Ness et al., 2016). The structure of the dendritic tree has also been implicated in the generation of LFP signals (Lindén et al., 2010). Results in the present work suggest that the biophysics of the axon and the site of the action potential initiation may be additional factors determining the amplitude and the spectrum of the extracellular potential. The effects of the AIS position on LFP generated from a network of multi-compartmental model neurons is an interesting outlook of the present work.

Acknowledgements

Research supported by the CNRS, the European Union (Human Brain Project H2020-720270), and the Agence Nationale de la Recherche (ANR-14-CE13-0003). MT was supported by Ecole des Neurosciences de Paris (ENP, http://www.paris-neuroscience.fr/) and DIM Cerveau et Pensée (http://dimcerveaupensee.fr/).

References

Barthó, P., Hirase, H., Monconduit, L., Zugaro, M., Harris, K. D., and Buzsáki, G. (2004). Characterization of neocortical principal cells and interneurons by network interactions and extracellular features. *Journal of neurophysiology*, 92(1):600–608.

Barthó, P., Hirase, H., Monconduit, L., Zugaro, M., Harris, K. D., and Buzsáki, G. (2004). Characterization of neocortical principal cells and interneurons by network interactions and extracellular features. *Journal of Neurophysiology*, 92(1):600–608.

Bédard, C., Kröger, H., and Destexhe, A. (2004). Modeling extracellular field potentials and the frequency-filtering properties of extracellular space. *Biophysical journal*, 86(3):1829–1842.

Brette, R. (2013a). Sharpness of spike initiation in neurons explained by compartmentalization. *PLoS computational biology*, 9(12).

Brette, R. (2013b). Sharpness of Spike Initiation in Neurons Explained by Compartmentalization. *PLoS Computational Biology*, 9(12):e1003338.

Dehghani, N., Peyrache, A., Telenczuk, B., Van Quyen, M. L., Halgren, E., Cash, S. S., Hatsopoulos, N. G., and Destexhe, A. (2016). Dynamic balance of excitation and inhibition in human and monkey neocortex. *Scientific Reports*, 6(23176):1–12.

Einevoll, G. T., Franke, F., Hagen, E., Pouzat, C., and Harris, K. D. (2012). Towards reliable spike-train recordings from thousands of neurons with multielectrodes. *Current Opinion in Neurobiology*, 22(1):11–17.

Evans, M. D., Dumitrescu, A. S., Kruijssen, D. L. H., Taylor, S. E., and Grubb, M. S. (2015). Rapid modulation of axon initial segment length influences repetitive spike firing. *Cell Reports*, 13(6):1233–1245.

Evans, M. D., Sammons, R. P., Lebron, S., Dumitrescu, A. S., Watkins, T. B., Uebele, V. N., Renger, J. J., and Grubb, M. S. (2013). Calcineurin signaling mediates activity-dependent relocation of the axon initial segment. *Journal of Neuroscience*, 33(16):6950–6963.

Fried, S. I., Lasker, A. C. W., Desai, N. J., Eddington, D. K., and Rizzo, J. F. (2009). Axonal sodium-channel bands shape the response to electric stimulation in retinal ganglion cells. *Journal of neurophysiology*, 101:1972–1987.

Gold, C., Henze, D. A., Koch, C., and Buzsáki, G. (2006). On the origin of the extracellular action potential waveform: A modeling study. *Journal of Neurophysiology*, 95:3113–3128.

Griffiths, D. (1999). *Introduction to Electrodynamics*. Prentice Hall.

Grubb, M. S. and Burrone, J. (2010). Activity-dependent relocation of the axon initial segment fine-tunes neuronal excitability. *Nature*, 465(7301):1070–4.

Hallermann, S., de Kock, C. P. J., Stuart, G. J., and Kole, M. H. P. (2012). State and location dependence of action potential metabolic cost in cortical pyramidal neurons. *Nature Neuroscience*, 15(7):1007–1014.

Hamada, M. S., Goethals, S., de Vries, S. I., Brette, R., and Kole, M. H. P. (2016). Covariation of axon initial segment location and dendritic tree normalizes the somatic action potential. *Proceedings of the National Academy of Sciences*, 113(51):14841–14846.

Hines, M. L. and Carnevale, N. T. (1997). The neuron simulation environment. *Neural computation*, 9(6):1179–1209.

Hines, M. L., Davison, A. P., and Muller, E. (2009). NEURON and Python. *Frontiers in Neuroinformatics*, 3:1.

Hinman, J. D., Rasband, M. N., and Carmichael, S. T. (2013). Remodeling of the axon initial segment after focal cortical and white matter stroke. *Stroke*, 44(1):182–189.

Holt, G. R. (1997). *A critical reexamination of some assumptions and implications of cable theory in neurobiology*. PhD thesis, California Institute of Technology.

Jun, J. J., Steinmetz, N. A., Siegle, J. H., Denman, D. J., Bauza, M., Barbarits, B., Lee, A. K., Anastassiou, C. A., Andrei, A., Aydin, Ç., Barbic, M., Blanche, T. J., Bonin, V., Couto, J., Dutta, B., Gratiy, S. L., Gutnisky, D. A., Häusser, M., Karsh, B., Ledochowitsch, P., Lopez, C. M., Mitelut, C.,

Musa, S., Okun, M., Pachitariu, M., Putzeys, J., Rich, P. D., Rossant, C., Sun, W. L., Svoboda, K., Carandini, M., Harris, K. D., Koch, C., O'Keefe, J., and Harris, T. D. (2017). Fully integrated silicon probes for high-density recording of neural activity. *Nature*, 551(7679):232–236.

Kuba, H., Ishii, T. M., and Ohmori, H. (2006). Axonal site of spike initiation enhances auditory coincidence detection. *Nature*, 444(7122):1069–1072.

Lewicki, M. S. (1998). A review of methods for spike sorting: the detection and classification of neural action potentials. *Network*, 9(4):R53–78.

Lindén, H., Pettersen, K. H., and Einevoll, G. T. (2010). Intrinsic dendritic filtering gives low-pass power spectra of local field potentials. *Journal of Computational Neuroscience*, 29(3):423–444.

McCormick, D. A., Connors, B. W., Lighthall, J. W., and Prince, D. a. (1985). Comparative electrophysiology of pyramidal and sparsely spiny stellate neurons of the neocortex. *Journal of neurophysiology*, 54(4):782–806.

Milstein, J. N. and Koch, C. (2008). Dynamic moment analysis of the extracellular electric field of a biologically realistic spiking neuron. *Neural computation*, 20(8):2070–2084.

Muir, J. and Kittler, J. T. (2014). Plasticity of GABAA receptor diffusion dynamics at the axon initial segment. *Frontiers in cellular neuroscience*, 8(June):151.

Naundorf, B., Wolf, F., and Volgushev, M. (2007). Neurophysiology: Hodgkin and Huxley model - still standing? *Nature*, 445(7123):E2–E3.

Ness, T. V., Remme, M. W. H., and Einevoll, G. T. (2016). Active subthreshold dendritic conductances shape the local field potential. *Journal of Physiology*, 0(1):1–31.

Nunez, P. L. and Cutillo, B. A. (1995). *Neocortical dynamics and human EEG rhythms*. Oxford University Press, USA.

Peyrache, A., Dehghani, N., Eskandar, E. N., Madsen, J. R., Anderson, W. S., Donoghue, J. A., Hochberg, L. R., Halgren, E., Cash, S. S., and Destexhe, A. (2012). Spatiotemporal dynamics of neocortical excitation and inhibition during human sleep. *PNAS*, 109(5):1731–1736.

Reimann, M. W., Anastassiou, C. a., Perin, R., Hill, S. L., Markram, H., and Koch, C. (2013). A biophysically detailed model of neocortical local field potentials predicts the critical role of active membrane currents. *Neuron*, 79(2):375–90.

Schafer, D. P., Jha, S., Liu, F., Akella, T., McCullough, L. D., and Rasband, M. N. (2009). Disruption of the axon initial segment cytoskeleton is a new mechanism for neuronal injury. *Journal of neuroscience*, 29(42):13242–13254.

Stegeman, F., Van Oosterom, A., and Colon, E. J. (1987). Far-field evoked potential components induced by a propagating generator: computational

evidence. *Electroencephalography and Clinical Neurophysiology*, 67(2):176–187.

Stevenson, I. H. and Kording, K. P. (2011). How advances in neural recording affect data analysis. *Nature Neuroscience*, 14(2):139–142.

Stuart, G., Schiller, J., and Sakmann, B. (1997a). Action potential initiation and propagation in rat neocortical pyramidal neurons. *Journal of Physiology*, 505(3):617–632.

Stuart, G., Spruston, N., Sakmann, B., and Häusser, M. (1997b). Action potential initiation and backpropagation in neurons of the mammalian cns. *Trends in neurosciences*, 20(3):125–131.

Telenczuk, B., Baker, S. N., Kempter, R., and Curio, G. (2015). Correlates of a single cortical action potential in the epidural EEG. *NeuroImage*, 109:357–367.

Telenczuk, B. and Telenczuk, M. (2016). NeuronEAP library. *Zenodo*, 10.5281/zenodo.49560.

Telenczuk, M., Fontaine, B., and Brette, R. (2017). The basis of sharp spike onset in standard biophysical models. *PLOS ONE*, 12(4):1–27.

Vigneswaran, G., Kraskov, A., and Lemon, R. N. (2011). Large Identified Pyramidal Cells in Macaque Motor and Premotor Cortex Exhibit "Thin Spikes": Implications for Cell Type Classification. *Journal of Neuroscience*, 31(40):14235–14242.

Wilson, M. and Bower, J. M. (1992). Cortical oscillations and temporal interactions in a computer simulation of piriform cortex. *Journal of Neurophysiology*, 67(4):981–995.

Yu, Y., Shu, Y., and McCormick, D. A. (2008). Cortical action potential backpropagation explains spike threshold variability and rapid-onset kinetics. *The Journal of neuroscience*, 28(29):7260–72.

Figures

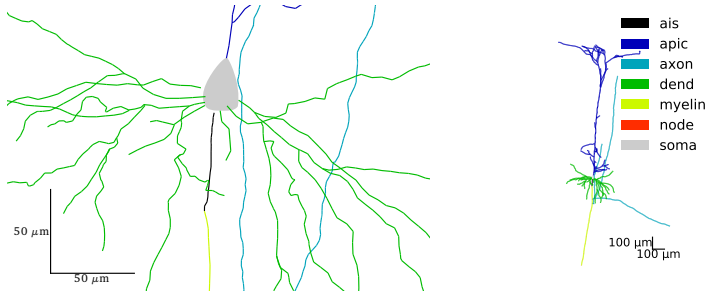

Figure 1: Morphology of the full compartmental model. Left: zoom in into the AIS

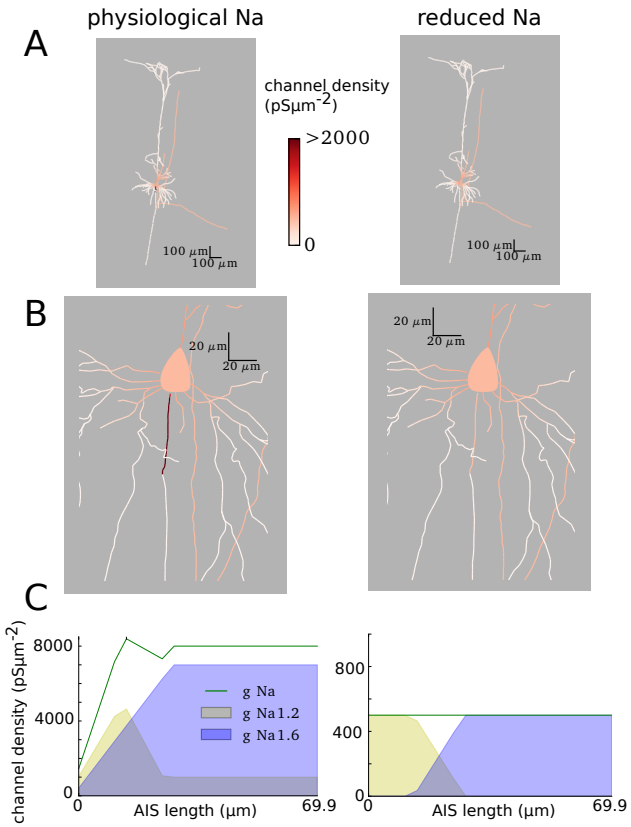

Figure 2: Sodium distribution within the neuron. Colorscale shows the density ($pS\mu m^{-2}$). **Left**: Physiological Na model, **Right**: Reduced Na model. **A**. full morphology. **B**. Zoom in into the soma and the initial segments of the axon. **C**. Concentrations of two different types of sodium cahhenls(Na and Nax) in the AIS (at 0 μm AIS is attached to the soma, 69.90 μm is its far end). Note that in both models, the density of Na channels in the soma is 500 $pS\mu m^{-2}$ while there are no Nax channels

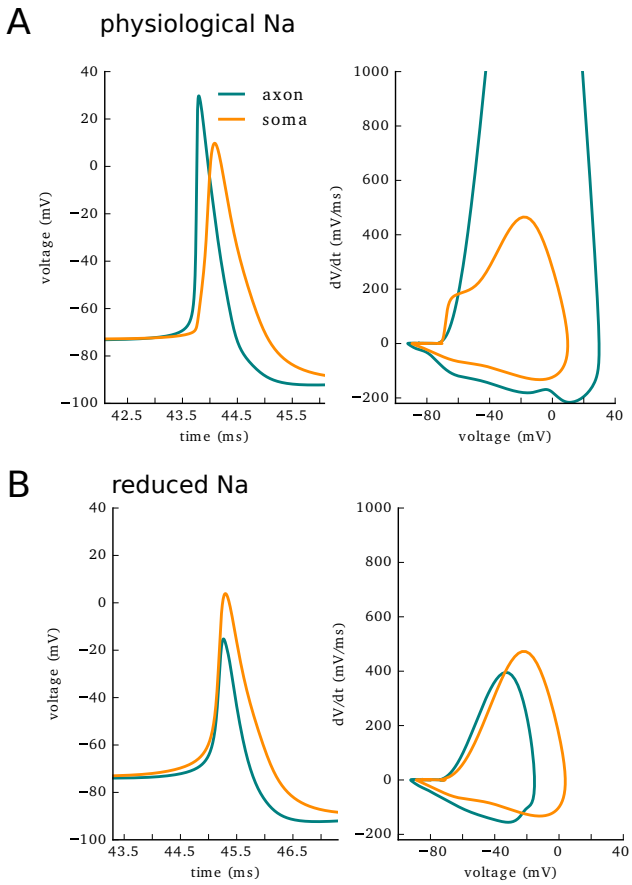

Figure 3: Action potentials in two different locations: soma (orange) and AIS (blue) (location where action potential initiates in the physiological Na model). **Left**: Time–voltage relationship and **Right**: change of voltage (phase-plot). **A**. Physiological Na model. **B**. Reduced Na model.

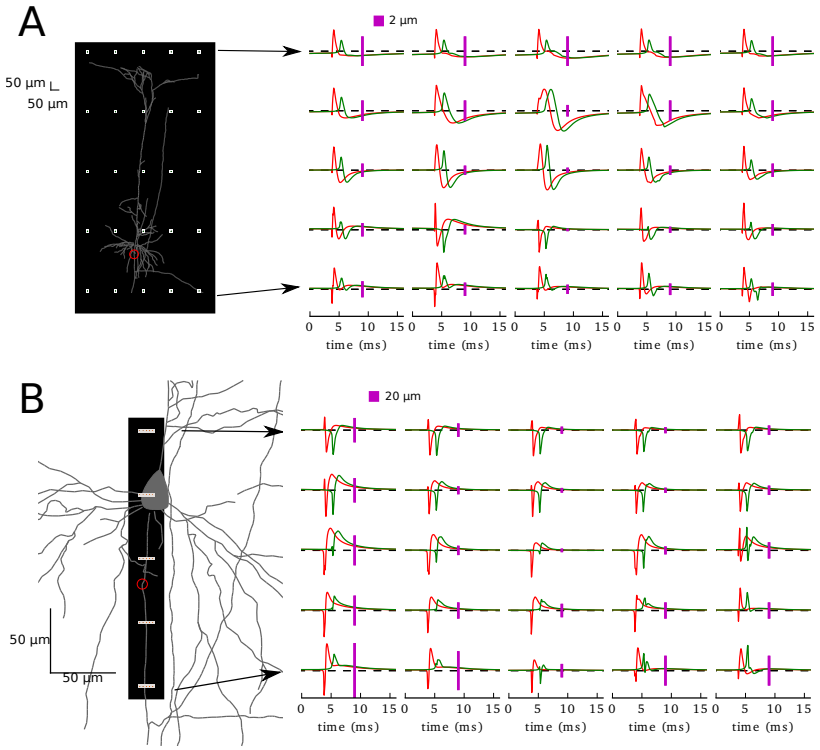

Figure 4: Local field potential (left) measured at different locations (white dots within the black rectangle) for the physiological Na model (red) and reduced Na model (green). Scale is shown in pink. **A**. Full morphology and **B**, zoom in to the soma and initial part of the axon. Axon initial segment (red circle).

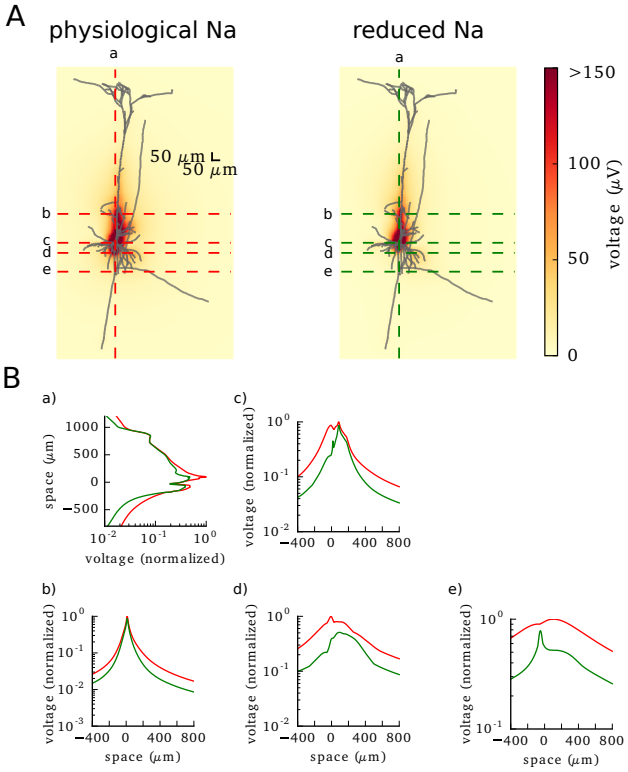

Figure 5: Maximum peak to peak amplitude of the signal calculated in the different places of the field. **A**. Full morphology imposed on the generated potential maximum amplitude (colorscale) in the physiological Na model (left) and reduced Na model (right). Dotted lines show where a-e are calculated in B. **B**. Maximum peak to peak potential normalized to the largest value of the signal generated by either of the models. Voltage is given in the logarithmic scale. (a) Signal recorded in the vertial axis passing through the soma, (b) signal recorded in the horizontal axis passing 200 μm above the soma, (c) signal recorded in the horizontal axis passing through the soma, (d) signal recorded in the horizontal axis passing through the AIS, (e) signal recorded in the horizontal axis passing through 200 μm below the soma.

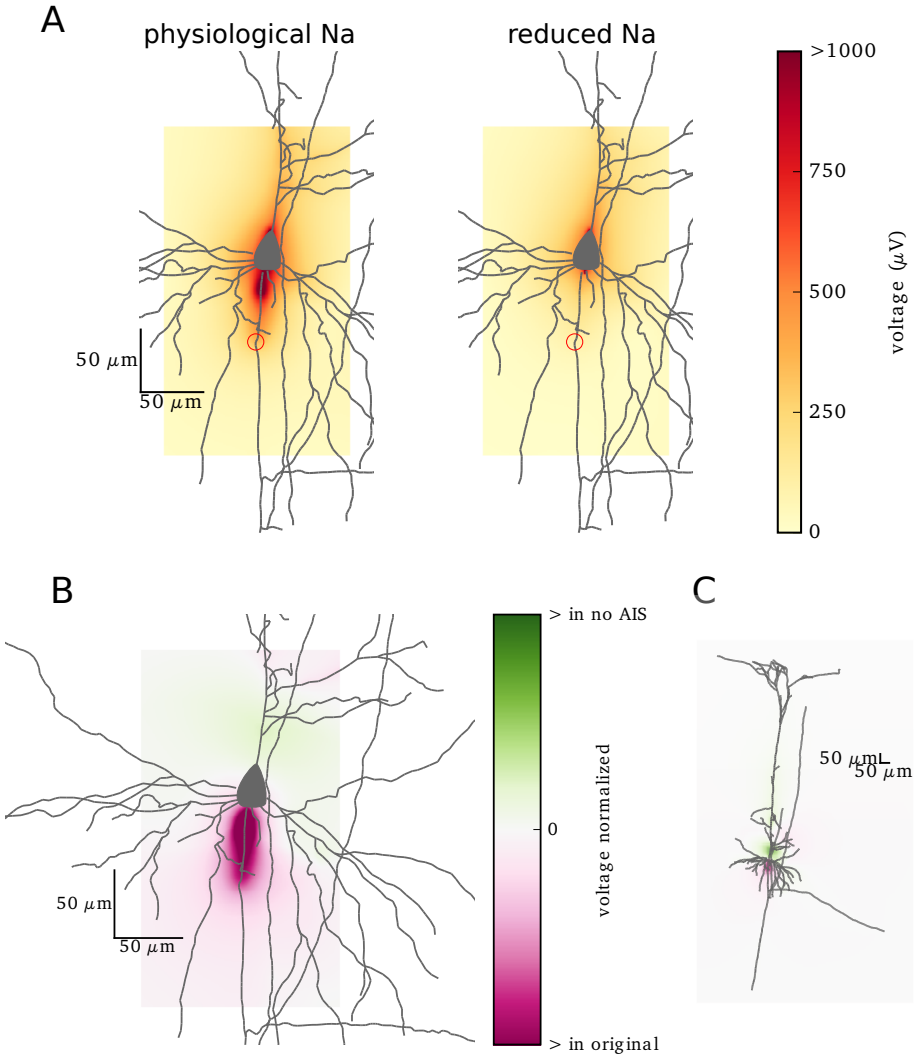

Figure 6: **A**. Zoom in to the maximum peak to peak of the local field potential generated by the physiological Na model (left) and reduced Na model (right). **B**. difference between normalized peak to peak amplitudes of the local field potential in the zoomed in view and **C** full morphology.

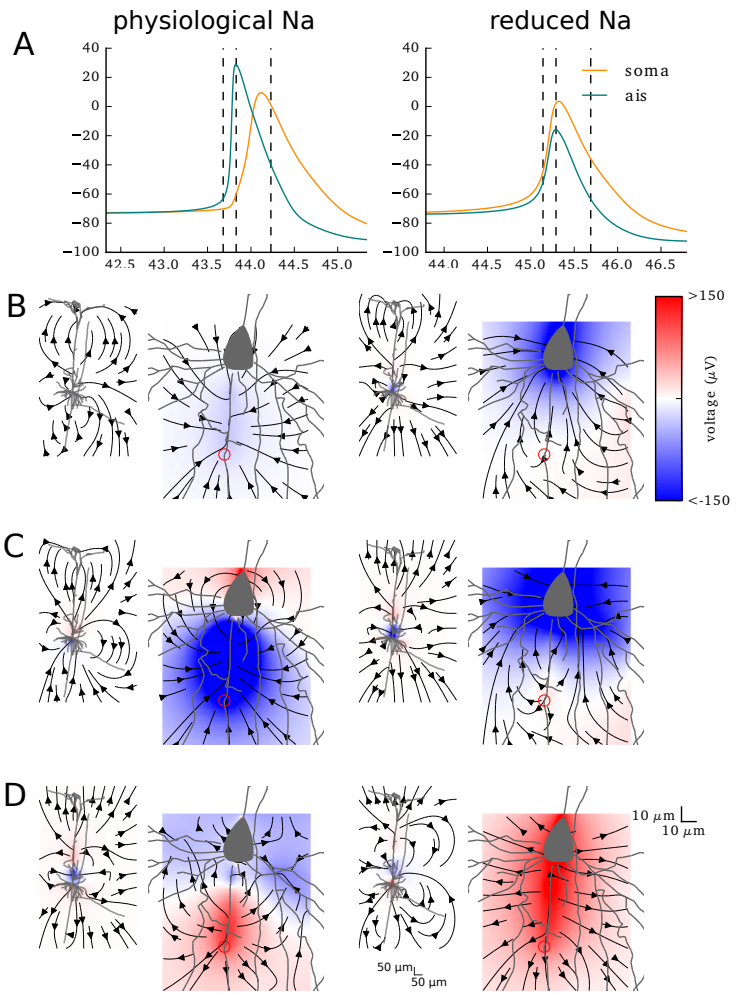

Figure 7: Local field potential at different time points of the action potential in the physiological Na model (left) and reduced Na model (right). **A**. Action potentials in the soma (orange) and in the end of the AIS (blue). Dotted vertical lines show at which time B-D are recorded. **B–D**. extracellular potential (colors) and electrical field (arrows) at different times of action potentials in zoomed-in view and full morphology (inset). Recordings were made at: 0.15 ms before the peak of the action potential in the AIS (B), at the peak of the action potential in the AIS (C), 0.4 ms after the peak of the AIS (D)

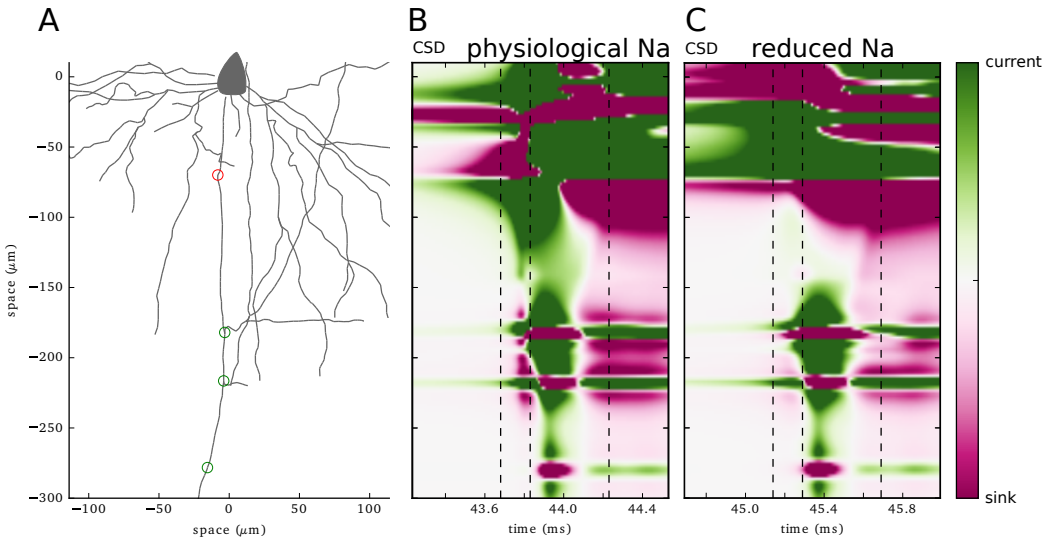

Figure 8: Current source density (CSD) during the action potential. **A**. Morphology zoomed-in to the soma, axon initial segment (the most distal part of AIS, red circle) and the first 3 nodes of ranvier (NoR, green circles). **B**. CSD calculated in the physiological Na model and **C** reduced Na model centered on the peak of the action potential in the AIS (middle vertical line). The three vertical lines correspond to the times of the action potential as in Fig. 7.

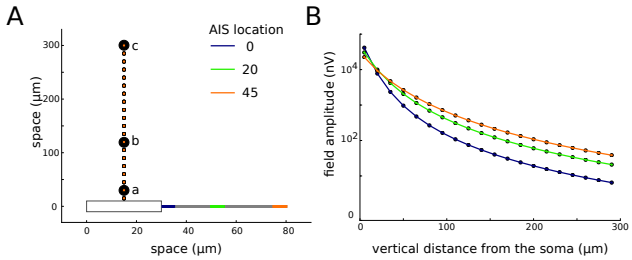

Figure 9: Extracellular potential calculated from the soma-axon model with the AIS at three different positions: 0 μm from the soma (blue), 20 μm from the soma (green) and 45 μm from the soma (orange). **A**. Each dot represents the location of the measurement vertically from the soma. Black circles correspond to the locations of recordings shown in C. Schematics shows the cell body (left) and the axon (grey) with the AIS at different locations (color-coded). **B**. Double logarithmic plot of the peak-to-valley amplitude of the extracellular potential vs the distance of the recording site from the soma. Color lines correspond to different positions of the AIS (see color code in A).

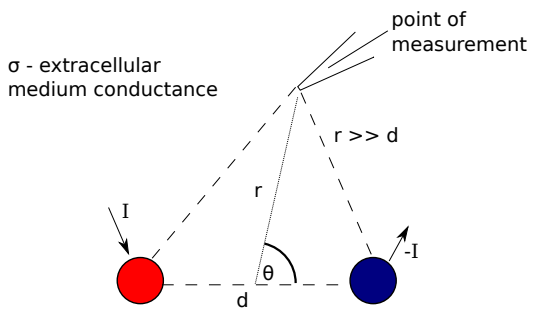

Figure 10: Dipole model consisting of a current sink (red) and a current source (blue) seperated by d. Point of measurement represents a possible recording location. For the far-field approximation to hold, the distance between the sink and source should be much smaller than the distance to the recording point. See text for more detail.

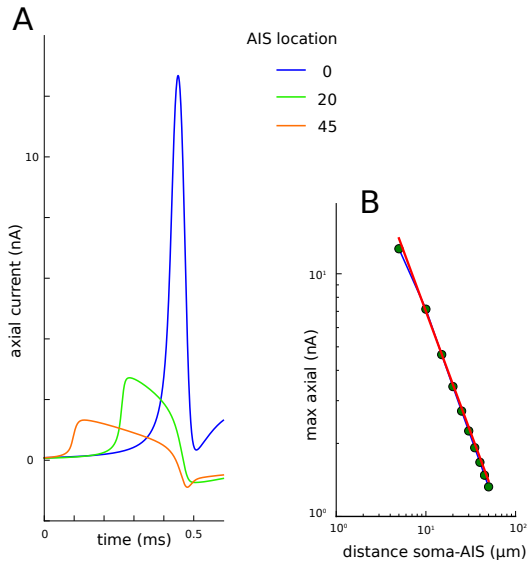

Figure 11: Dependence of axial current amplitude on the distance between the soma and the AIS in the soma-axon model. **A**. Axial current passing from the axon to the soma during the action potential, shifted to the peak of somatic spike, **B**. The maximum of axial current vs the distance of the AIS end proximal to the soma in double-logarithmic scale. Red line shows the fitted function $I = (70\,\mathrm{nA} \cdot \mu\mathrm{m})/d$ (which is a linear function in double-logarithmic scale).

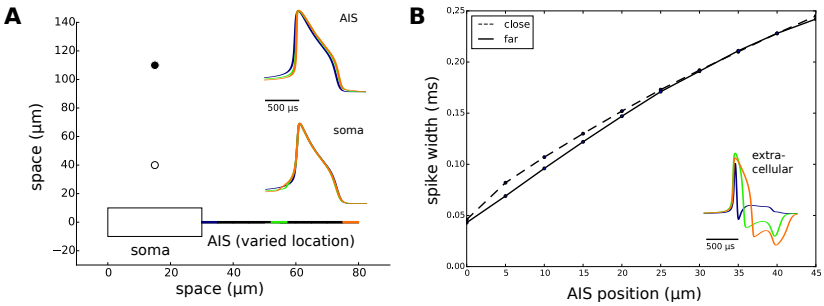

Figure 12: Width of the extracellular AP as a function of the soma-AIS separation. **A**. Schematic representation of the soma-axon model (bottom) and their relation to the recording points (dots above soma). The AIS position was systematically varied from 0 (directly attached to the soma) to 45 μm. Insets: Waveforms of action potentials recorded intracellularly in the AIS (top inset) and the soma (bottom). **B**. Action potential width measured at half amplitude as a function of the AIS position for two different recording locations (close: 30 μm from soma, far: 100 μm from soma). Inset: Examples of extracellular AP waveshapes for 3 different locations of AIS (recorded 40 μm above the soma).